Weak interlayer dependence of lattice thermal conductivity on stacking thickness of penta-graphene

Fancy Qian Wang, Jie Liu, Xiaoyin Li, Qian Wang, and Yoshiyuki Kawazoe

Citation: Appl. Phys. Lett. **111**, 192102 (2017);
View online: https://doi.org/10.1063/1.4996054
View Table of Contents: http://aip.scitation.org/toc/apl/111/19
Published by the American Institute of Physics

Weak interlayer dependence of lattice thermal conductivity on stacking thickness of penta-graphene

Fancy Qian Wang,[1] Jie Liu,[1] Xiaoyin Li,[1] Qian Wang,[1,a)] and Yoshiyuki Kawazoe[2,3]
[1]*Center for Applied Physics and Technology, College of Engineering, Peking University, Beijing 100871, China and Key Laboratory of High Energy Density Physics Simulation, Ministry of Education, Beijing 100871, China*
[2]*New Industry Creation Hatchery Center, Tohoku University, Sendai 980-8577, Japan*
[3]*Physics and Nanotechnology, Sri Ramaswamy Memorial University, Kattankulathur 603203 TN, India*

(Received 14 July 2017; accepted 24 October 2017; published online 6 November 2017)

Penta-graphene (PG), as a novel carbon allotrope, has attracted considerable attention because of its unique atomic structure and outstanding intrinsic properties. Here, we systematically investigate the effect of layer numbers on the lattice thermal conductivity of the stacked PG structures by solving exactly the linearized phonon Boltzmann transport equation combined with first-principles calculations. We find that the lattice thermal conductivity of the stacked PG is insensitive to the number of layers, which is in sharp contrast to that of graphene. Such a layer-independent thermal conductivity is attributed to the buckled structure of PG which breaks the two-dimensional selection rule of three-phonon scattering and the weak van der Waals interlayer interactions that hardly have any effect on the lattice thermal conductivity. This mechanism can be generalized to other van der Waals layered materials with buckled or puckled structures, which may also show the layer-independent lattice thermal conductivity. *Published by AIP Publishing.* https://doi.org/10.1063/1.4996054

Since the successful synthesis of graphene,[1] extensive research interest has been triggered in exploring novel carbon-based nanomaterials because of their fantastic properties[2–5] and great potential in technological applications.[6–9] Recently, a new carbon allotrope named penta-graphene (PG) was proposed.[10] Its unique atomic configuration and exceptional properties, such as an intrinsic quasi-direct bandgap, negative Poisson's ratio, and ultrahigh ideal strength, have not only motivated the study of other pentagon-based two-dimensional (2D) structures,[11–17] enriching the family of uiltrathin 2D materials, but also led to the further investigation of the potential applications of PG in nanoelectronics,[18,19] optical devices,[20] Li/Na-ion batteries,[21] and catalysts.[22]

Thermal conductivity is an important physical parameter used to assess the heat dissipation ability of materials. Usually, materials with high thermal conductivity are desirable in electronic applications for better performance and longer lifetimes of devices.[23] In this aspect, PG with a relatively high lattice thermal conductivity κ_{lat} of 645 W/mK[24] is attractive, as it could be used as a thermal management material for cooling electronic devices. Meanwhile, it has been demonstrated that some external factors such as chemical functionalization and tensile strain have a significant influence on the κ_{lat} of PG. For instance, the κ_{lat} increases notably (76%) *via* hydrogenation due to the weak bonding anharmonicity in the hydrogenated PG,[25] while it monotonically decreases when stretched.[26] In addition, it has been reported that vertically stacking 2D sheets *via* van der Waals interactions is another possible way to tune thermal conductivity, and the number of the stacked layers play a role in tuning the lattice thermal conductivity in some cases. The in-plane κ_{lat} can show complicated behaviours in layer dependence for 2D materials with different compositions or in different environments.[27,28] For example, the in-plane κ_{lat} of mutilayer graphene and hexagonal boron nitride (h-BN) decreases significantly as compared to that of their monolayer counterpart, mainly due to the breaking of the 2D selection rule of three-phonon scattering.[29–31] However, for supported mutilayer graphene, the κ_{lat} is found to increase rapidly with the layer thickness, reaching about 90% of that of bulk graphite at six layers.[32] While for multilayer phosphorene, the in-plane κ_{lat} is insensitive to the number of layers, because the behavior of out-of-plane phonon modes is hindered due to their puckered structures.[33] In addition, the influence of the MoS_2 layer thickness on its in-plane κ_{lat} is still under debate with the consideration of the quite different results obtained by previous studies.[34–36] These findings motivate us to explore the lattice thermal conductivity of the stacked PG structures that are unreported so far. We wondered how the thermal transport changes with the layer numbers. In this paper, we systematically study the effect of the layer numbers on the lattice thermal conductivity of the stacked PG structures.

In semiconductors, heat is carried primarily by phonons and the intrinsic lattice thermal conductivity κ_{lat} is dominated by phonon-phonon interactions resulting from the anharmonicity of interatomic potential around and above room temperature.[30,37] The microscopic description of κ_{lat} as the sum of contributions over all the phonon modes λ ($\boldsymbol{q}$, j) with the wave vector $\boldsymbol{q}$ and branch index j is derived from the phonon Boltzmann transport equation (BTE)[38] given as

$$\kappa_{lat}^{\alpha\beta} = \frac{1}{(2\pi)^2 (n\delta)} \sum_{\lambda} \frac{\partial f}{\partial T} (\hbar\omega_{\lambda})^2 \nu_{\lambda}^{\alpha} \nu_{\lambda}^{\beta} \tau_{\lambda}, \tag{1}$$

where n is the number of uniformly spaced $\boldsymbol{q}$ points in the Brillouin zone, f is the Bose distribution function, ω_{λ} is the

a)E-mail: qianwang2@pku.edu.cn

frequency of a phonon mode λ ($\boldsymbol{q}$, j), $\nu_\lambda^\alpha(\nu_\lambda^\beta)$ is the component of the phonon velocity along the thermal transport direction α (β), τ_λ is the phonon lifetime of each phonon mode, and δ is the interlayer distance, which is set as 3.704 Å for 1- and ∞-layered penta-graphene while 7.408 Å for 2-layered penta-graphene. The layer number N of PG is limited to 1, 2, and ∞ (corresponding to the period system), which are good enough for the conclusion.

The phonon lifetime τ_λ is determined using an iterative approach, as implemented in the ShengBTE package,[39] which solves exactly the linearized phonon Boltzmann transport equation (BTE). This method has been widely used to calculate the κ_{lat} of various materials, showing satisfactory accuracy and predictive power.[40–42] For the inputs to the BTE, a series of harmonic and anharmonic interatomic force constants (IFCs) are required, which are obtained from first-principles calculations within the framework of density functional theory (DFT) as implemented in the Vienna *Ab initio* Simulation Package (VASP).[43] To accurately describe the dispersion force and obtain the interlayer distance, the structures of the N-layered PG are optimized using optB88-vdW functional.[44,45] The kinetic energy cutoff of the plane waves with a value of 500 eV and the cutoff radius up to the 14th nearest neighbors are selected for all the systems studied here. The $8 \times 8 \times 1$ ($6 \times 6 \times 1$ and $6 \times 6 \times 3$) and $5 \times 5 \times 1$ ($4 \times 4 \times 1$ and $4 \times 4 \times 4$) supercells of 1-layered (2- and ∞-layered) PG are constructed and used to calculate the harmonic and anharmonic IFCs, respectively. In addition, the isotopic impurity scattering and boundary scattering at the diffusive limits ($L \to \infty$) are also included in our calculations.

Although multilayer 2D materials can be constructed by stacking their monolayers, the stacking alignment is difficult to be controlled in real fabrication processes, especially for the multilayer structures fabricated by using direct transfer technology.[46] Here, we consider several possible stacking patterns of the 2-layered PG according to the stacking misalignment (SM) rule.[19,47,48] First, we perform calculations by varying the SM from 0 (ideal 2-layered AA-stacking) to 1/2 a (AB-stacking) with an interval of 1/8 a, where $a = 3.64$ Å is the optimized lattice constants of the monolayer PG. Unlike graphene, which favors the AB-stacking, our total-energy calculations based on the optB88-vdW functional indicate that the AA-stacking penta-graphene is the most energetically favorable structure, as shown in Fig. 1(a). Then, we take the other two stacking patterns into account, which possess high symmetry and are built based on the AA-stacking, as shown in Figs. 1(b) and 1(c), respectively. The $AA_{1/4}$-stacking can be viewed as shifting the top layer of the AA-stacking by $(\sqrt{2}/2)$ a along the diagonal direction. While for the AA′-stacking, the top and bottom layers are mirror images of each other. However, the stacking order still prefers the AA-stacking with the lowest total energy. Therefore, we only focus on the structure with the AA-stacking arrangement in the following discussions. For the 2-layered PG, the optimized lattice constants are $a = b = 3.643$ Å. At the equilibrium distance between the two layers, we calculate the binding energy (E_b) per carbon atom, which is defined as $E_b = (E_{2\text{-layer}} - 2E_{\text{single}})/M$, where $E_{2\text{-layer}}$ is the total energy of the optimized 2-layered PG, E_{single} is the total energy of the isolated PG sheet, and $M = 12$ is the number of carbon atoms in a unit cell of the 2-layered PG. The calculated binding energy of the 2-layered PG is 34 meV/atom with an optimized distance of 2.486 Å, which has the same order of magnitude as that of other van der Waals (vdW) bilayer systems such as bilayer graphene ($E_b = 50$ meV/atom),[49] the vdW heterostructure formed by graphene and phosphorene ($E_b = 60$ meV/atom),[49] and MoS_2 and graphene heterobilayers ($E_b = 58$ meV/atom).[50]

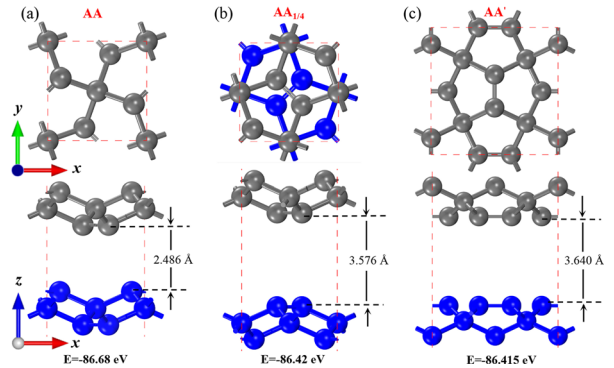

FIG. 1. Top and side views of the optimized structures of the 2-layered PG with different stacking patterns: (a) AA-stacking, (b) $AA_{1/4}$-stacking, and (c) AA′-stacking. The top and bottom layers are in gray and blue, respectively. The corresponding total energy and optimized interlayer distance are also given.

Since the phonon spectrum carries the important information on the vibrational states, we then turn our attention to study the lattice dynamics of the N-layered PG. Our focus is on the low frequency part of the phonon spectrum (<16 THz), because in this region, the phonon dispersions of the 2- and ∞-layered PG are different from that of the PG monolayer. In addition, the Γ-X direction (the in-plane direction) is chosen as the typical high symmetry path, as the contribution to thermal conductivity along this direction weakly depends on the phonon dispersion along other directions. We can see that the N-layered PG all have three acoustic branches including the in-plane linear transverse acoustic mode (TA_1), longitudinal acoustic mode (LA_1), and the out-of-plane flexural acoustic mode (ZA_1), as shown in Fig. 2. While for the 2-layered PG, the weak interlayer coupling produces another three low-lying optical phonon branches for each acoustic branch (TA_1, LA_1, and ZA_1), which are labeled as TA_2, LA_2, and ZA_2 [see Fig. 2(b)], respectively. We find that the TA_2 and LA_2 branches deviate from the TA_1 and LA_1 just in the region around the Γ point, whereas the flexural mode ZA_2 deviates significantly from the ZA_1

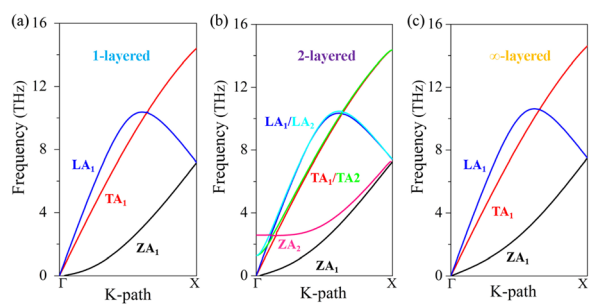

FIG. 2. Phonon spectrum of the acoustic and low-lying optical branches along the Γ-X high symmetry line for (a) 1-layered, (b) 2-layered, and (c) ∞-layered PG.

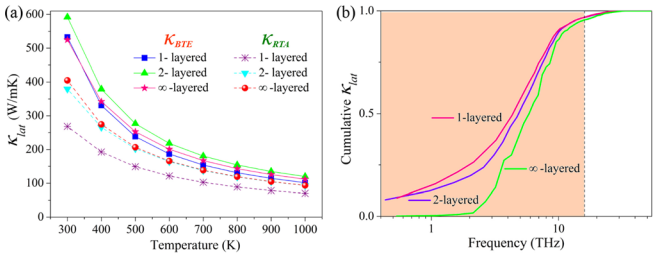

FIG. 3. (a) Variation of the lattice thermal conductivity κ_{lat} at different temperatures calculated using both the solution of linearized BTE and RTA. (b) Normalized cumulative κ_{lat} as a function of frequency for *N*-layered penta-graphene. The low-frequency range (<16 THz) is marked in orange.

mode throughout the Brillouin zone. However, such a discrepancy of the ZA mode in the 2-layered PG is smaller than that of 2-layered graphene: at the Γ point, the split of the ZA mode is about 2.5 THz in 2-layered penta-graphene, while increases to 9 THz in 2-layered graphene.[30] Such features indicate that the interlayer coupling of penta-graphene is even weaker than that of graphene, thus offering opportunities for penta-graphene to have a layer-independent κ_{lat}. Besides, we note that the ZA_i modes of ∞-layered PG do not look like a continuum, which is quite different from that of graphene because of the different stacking patterns between PG (AA) and graphene (AB).

In order to examine the effect of layer numbers on the lattice thermal conductivity, we perform first-principles calculations on the in-plane lattice thermal conductivity κ_{lat} of the *N*-layered PG ($N = 1,2, \infty$) as a function of temperature, using both the solution of the linearized BTE and single-mode relaxation time approximation (RTA).[51] The results are given in Fig. 3(a), which shows that the calculated κ_{lat} under the RTA (κ_{RTA}) is much smaller than that obtained by using the solution of the linearized BTE (κ_{BTE}). The reason is that, within the RTA solution, the Normal scattering process is incorrectly treated as an independent resistive process on the same footing as the Umklapp scattering process; hence, the κ_{RTA} always exhibits smaller magnitude as compared to the κ_{BTE}, especially in the materials with the strong Normal scattering process, as the cases in some other carbon allotropes.[30,52,53] In addition, the κ_{RTA} gradually approaches to the κ_{BTE} as the temperature increases because more high frequency branches are excited and involved in the Umklapp scattering processes, which dominates at high temperature. By using the solution of the linearized phonon BTE, the in-plane κ_{lat} of PG is found to be almost independent of the number of the PG layers especially at high temperature. The calculated κ_{lat} of 592 W/mK for the 2-layered PG is slightly larger than that of the monolayer (533 W/mK) and ∞-layered (525 W/mK) PG at 300 K. The calculated percentage of change is 11.2% and 11.4%, respectively, when *N* increases from 1 to 2 and from 2 to ∞ at 300 K for PG. While the corresponding percentage for graphene[29,30] is 28.9% and 11.5%. Obviously, PG shows a weaker interlayer dependence of κ_{lat} as compared to graphene. The possible reasons are the refection symmetry exists in the monolayer graphene along the in-plane direction, leading to a 2D selection rule of three-phonon scattering processes, which means that only even numbers of out-of-plane modes can be involved in the three-phonon scattering processes. Thus, sixty percent of scattering processes are forbidden in the monolayer graphene. However, the reflection symmetry is not preserved in the 2-layered graphene because of the interlayer coupling. So, the κ_{lat} of the 2-layered graphene is significantly reduced to about 20% of that of the monolayer graphene[30,54] due to breaking the 2D selection rule. In addition, the reduction of κ_{lat} slows down with increasing the layers, and the κ_{lat} converges to the value of graphite when increased to about five layers.[30] In this case, the weak and short ranged interlayer interaction rather than breaking selection rule is responsible for the reduction of κ_{lat}.[30] Accordingly, if the intrinsic structure of materials is not purely planar like PG, then the 2D selection rule held in monolayer graphene cannot be applied to them due to the lack of reflection symmetry. Furthermore, we have mentioned that the interlayer interaction between the PG layers is even weaker than that of graphene, thus hardly affecting its κ_{lat}. Consequently, the effect of the layer numbers is subtle in these buckled structures. In addition, under the RTA solution, the κ_{lat} of ∞-layered PG is comparable to that of the 2-layered PG, while smaller than that of the PG monolayer in the whole temperature range, indicating that the Normal scattering process weakens with adding the layers.

To figure out the main heat carriers in the *N*-layered PG, the normalized cumulative κ_{lat} as a function of frequency is calculated. The results are plotted in Fig. 3(b), which shows that κ_{lat} of the *N*-layered PG is dominantly contributed by the phonons with frequencies lower than 16 THz, indicating that the acoustic and low-lying optical phonon branches carry the majority of the heat, similar to that of graphene. Therefore, we focus on the low frequency branches (<16 THz) in the later discussions.

To confirm that the κ_{lat} of the *N*-layered PG is layer-independent, we further calculate the other two essential factors including the frequency-dependent phonon velocity V_g and the three-phonon scattering rate, which are critical for deciding the κ_{lat}. The calculated results are given in Figs. 4(a) and 4(b). From the V_g-ω relationship, one can see that the V_g is almost degenerate for the *N*-layered PG structures, making the κ_{lat} more possible to be layer-independent. On the other hand, the three-phonon scattering rate, which dominates the intrinsic κ_{lat} around and above room temperature, varies with the number of layers *N* in the range of high frequencies, where the PG monolayer possesses a slightly larger three-phonon scattering rate than that of 2- and ∞-layered PG. However, it should be mentioned that these high frequency branches have relatively small contributions to the κ_{lat} and thus cannot lead to a variation of κ_{lat}. Actually, these high-frequency branches mainly participate in the Normal scattering process, providing important scattering channels for the low-frequency branches, from which a large fraction of resistive Umklapp scattering derives.[42] To get the details, the Normal scattering rate for higher frequency branches (>16 THz) is calculated and plotted in Fig. 4(c). The results show that the Normal scattering rate of the PG monolayer is larger than that of the 2- and ∞-layered PG, which also gives a reasonable explanation to the results obtained under RTA with the order of κ_{lat} ($N = 1$) < κ_{lat} ($N = 2$) = κ_{lat} ($N = \infty$). Furthermore, we also compare the relative contributions of

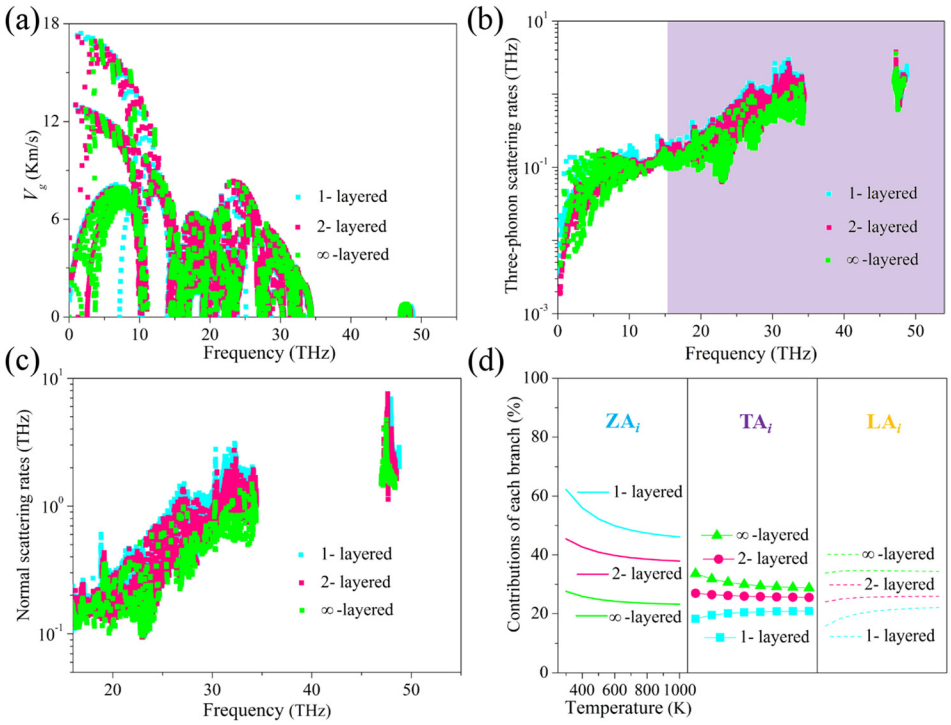

FIG. 4. Variation of the (a) group velocity V_g, (b) three-phonon scattering rates, and (c) Normal scattering rates with frequency. The high-frequency range (>16 THz) is marked in purple. (d) Contributions of the acoustic and the low-lying optical branches to κ_{lat} as a function of temperature for the N-layered PG.

the acoustic and the low-lying phonon branches to the κ_{lat} in the N-layered PG, as shown in Fig. 4(d). The ZA$_i$ (i = 1, 2, ∞) mode is much more sensitive to the variation of temperatures than the LA$_i$ and TA$_i$ modes, because the ZA$_i$ mode is in the lowest frequency range, and thus can be excited first at the given temperature. At 300 K, The contributions of the ZA$_i$ mode to κ_{lat} decrease from 62.3% to 45.5% and 27.6% with the layer number N increasing from 1 to 2 and ∞, respectively. On the contrary, the contributions of the LA$_i$ or TA$_i$ mode to κ_{lat} are slightly increased with adding the number of layers, as a consequence of the weak interlayer coupling.

The three phonon phase space P_3 contains the scattering events that satisfy energy and momentum conservation conditions and thus can be used to assess quantitatively the number of scattering channels.[39,55] The phase space available for the three phonon process including both the N and U processes is defined as $P_3 = \frac{2}{3\Omega}\left(P_3^+ + \frac{1}{2}P_3^-\right)$, where $P_3^{\pm} = \sum_j \int d\vec{q} D_j^{\pm}(\vec{q})$ and $D_j^{\pm}(\vec{q}) = \sum_{j'j''} \int d\vec{q}\delta\left[\omega_j(\vec{q}) \pm \omega_{j'}(\vec{q}') - \omega_{j''}(\vec{q} \pm \vec{q}'' - G)\right]$. Here, $D_j^{\pm}(\vec{q})$ corresponds to absorption (+) and emission processes (−), respectively. The available P_3 slightly changes from 1.38×10^{-3} to 1.33×10^{-3}, and 1.32×10^{-3} eV^{-1} for the l-, 2-, and ∞-layered PG, respectively, as displayed in Fig. 5(a). This feature also confirms that κ_{lat} is insensitive to the layer-number of the stacked PG structures. Meanwhile, we also examine the room-temperature cumulative κ_{lat} as a function of maximum mean free path allowed, i.e., the value of κ_{lat} when only phonons with a mean free path below a certain threshold are taken into account, as shown in Fig. 5(b). The results reveal that the N-layered PG possesses an extremely broad phonon mean free path spectrum ranging from a few nanometers to microns, showing the uneven contributions to κ_{lat} from different phonon branches.

What is more, although the PG shows weak interlayer dependence of κ_{lat} on the stacking thickness, we note that the 2-layered PG shows a slightly larger κ_{lat} than that of 1- and ∞-layered PG. The underlying reasons are (1) we have shown that the 1-layered PG possesses a slightly larger three-phonon scattering rate and three-phonon phase space *P3* than that of 2- and ∞-layered PG, leading to the relationship of κ_{lat} ($N = 1$) < κ_{lat} ($N = 2$) ≈ κ_{lat} ($N = \infty$); (2) For 2- and ∞-layered PG, we calculated their boundary scattering rates, as displayed in Fig. S1 in the supplementary material. One can see that, in the colored regions, the boundary scattering rates increase from $N = 2$ to $N = \infty$, and thus, there should have κ_{lat} ($N = 2$) > κ_{lat} ($N = \infty$). Therefore, these two factors (weaker phonon boundary scattering rates[36] and the reduced three-phonon phase space *P3*) result in the slight increase in κ_{lat} of 2-layered PG. Actually, the oscillating behavior displayed in PG has also been found in other 2D systems. For example, the multilayer phosphorene,[33] MoS_2 (Ref. 34), and h-BN[12] also exhibit oscillating behaviors between the κ_{lat} and N ($N = 1, 2, 3\ldots$), as displayed in Fig. S2 in the supplementary material.

In summary, we have investigated the dependence of the in-plane lattice thermal conductivity κ_{lat} on the layer number of the stacked PG by solving exactly the linearized phonon Boltzmann transport equation combined with the state-of-the-art first-principles calculations. Different from the case of graphene, the κ_{lat} of PG is insensitive to the variation of

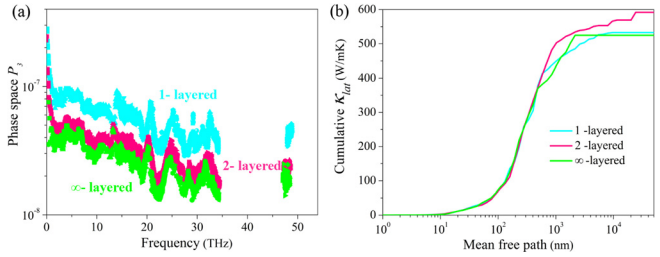

FIG. 5. (a) Frequency-dependent three-phonon phase space P_3 and (b) cumulative κ_{lat} as a function of the mean free path for the N-layered PG.

the number of layers. The main reason is that the buckled pentagonal structure of PG lacks the reflection symmetry, and thus, the 2D selection rule of three-phonon scattering valid for the planar structures such as graphene is no longer applicable. The further analysis of the three-phonon scattering rates, three-phonon phase space, phonon velocity, and phonon mean free path confirms our conclusions. The insensitivity of the in-plane lattice thermal conductivity to the stacking thickness offers an advantage over graphene, namely, no need to precisely control the stacking thickness of PG for its thermal performance.

See supplementary material for more information about the phonon boundary scattering rates for PG and the similar oscillating behaviors between κ_{lat} and N for other 2D materials.

This work was partially supported by grants from the National Natural Science Foundation of China (NSFC-51471004) and the National Key Research and Development Program of China (Grant No. 2016YFE0127300). The authors thank the crew of the Center for Computational Materials Science, the Institute for Materials Research, Tohoku University (Japan), for their continuous support of the HITACHI SR16000 supercomputing facility.

[1]K. S. Novoselov, A. K. Geim, S. V. Morozov, D. Jiang, Y. Zhang, S. V. Dubonos, I. V. Grigorieva, and A. A. Firsov, Science **306**, 666 (2004).
[2]Y. Zhang, Y.-W. Tan, H. L. Stormer, and P. Kim, Nature **438**, 201 (2005).
[3]C. Lee, X. Wei, J. W. Kysar, and J. Hone, Science **321**, 385 (2008).
[4]C. L. Kane and E. J. Mele, Phys. Rev. Lett. **95**, 226801 (2005).
[5]S. V. Morozov, K. S. Novoselov, M. I. Katsnelson, F. Schedin, D. C. Elias, J. A. Jaszczak, and A. K. Geim, Phys. Rev. Lett. **100**, 016602 (2008).
[6]K. S. Kim, Y. Zhao, H. Jang, S. Y. Lee, J. M. Kim, K. S. Kim, J.-H. Ahn, P. Kim, J.-Y. Choi, and B. H. Hong, Nature **457**, 706 (2009).
[7]F. Bonaccorso, Z. Sun, T. Hasan, and A. C. Ferrari, Nat. Photonics **4**, 611 (2010).
[8]F. Schwierz, Nat. Nanotechnol. **5**, 487 (2010).
[9]E. Yoo, J. Kim, E. Hosono, H.-S. Zhou, T. Kudo, and I. Honma, Nano Lett. **8**, 2277 (2008).
[10]S. Zhang, J. Zhou, Q. Wang, X. Chen, Y. Kawazoe, and P. Jena, Proc. Natl. Acad. Sci. U.S.A. **112**, 2372 (2015).
[11]Y. Ma, L. Kou, X. Li, Y. Dai, and T. Heine, NPG Asia Mater. **8**, e264 (2016).
[12]J. Li, X. Fan, Y. Wei, H. Liu, S. Li, P. Zhao, and G. Chen, Sci. Rep. **6**, 33060 (2016).
[13]J. I. Cerdá, J. Sławińska, G. Le Lay, A. C. Marele, J. M. Gómez-Rodríguez, and M. E. Dávila, Nat. Commun. **7**, 13076 (2016).
[14]M. Yagmurcukardes, H. Sahin, J. Kang, E. Torun, F. M. Peeters, and R. T. Senger, J. Appl. Phys. **118**, 104303 (2015).
[15]X. Li, Y. Dai, M. Li, W. Wei, and B. Huang, J. Mater. Chem. A **3**, 24055 (2015).
[16]F. Li, K. Tu, H. Zhang, and Z. Chen, Phys. Chem. Chem. Phys. **17**, 24151 (2015).
[17]A. Lopez-Bezanilla and P. B. Littlewood, J. Phys. Chem. C **119**, 19469 (2015).
[18]G. R. Berdiyorov, G. Dixit, and M. E. Madjet, J. Phys.: Condens. Matter. **28**, 475001 (2016).
[19]Z. G. Yu and Y.-W. Zhang, J. Appl. Phys. **118**, 165706 (2015).
[20]Z. Wang, F. Dong, B. Shen, R. J. Zhang, Y. X. Zheng, L. Y. Chen, S. Y. Wang, C. Z. Wang, K. M. Ho, Y.-J. Fan, B.-Y. Jin, and W.-S. Su, Carbon **101**, 77 (2016).
[21]B. Xiao, Y.-C. Li, X.-F. Yu, and J.-B. Cheng, ACS Appl. Mater. Interfaces **8**, 35342 (2016).
[22]R. Krishnan, W.-S. Su, and H.-T. Chen, Carbon **114**, 465 (2017).
[23]E. S. Toberer, L. L. Baranowski, and C. Dames, Annu. Rev. Mater. Res. **42**, 179 (2012).
[24]F. Q. Wang, J. Yu, Q. Wang, Y. Kawazoe, and P. Jena, Carbon **105**, 424 (2016).
[25]X. Wu, V. Varshney, J. Lee, T. Zhang, J. L. Wohlwend, A. K. Roy, and T. Luo, Nano Lett. **16**, 3925 (2016).
[26]H. Liu, G. Qin, Y. Lin, and M. Hu, Nano Lett. **16**, 3831 (2016).
[27]X. Xu, L. F. C. Pereira, Y. Wang, J. Wu, K. Zhang, X. Zhao, S. Bae, C. T. Bui, R. Xie, and J. T. L. Thong, Nat. Commun. **5**, 3689 (2014).
[28]X. Xu, J. Chen, and B. Li, J. Phys.: Condens. Matter **28**, 483001 (2016).
[29]D. Singh, J. Y. Murthy, and T. S. Fisher, J. Appl. Phys. **110**, 044317 (2011).
[30]L. Lindsay, D. A. Broido, and N. Mingo, Phys. Rev. B **83**, 235428 (2011).
[31]L. Lindsay and D. A. Broido, Phys. Rev. B **85**, 035436 (2012).
[32]J. Chen, G. Zhang, and B. Li, Nanoscale **5**, 532 (2013).
[33]Y.-Y. Zhang, Q.-X. Pei, J.-W. Jiang, N. Wei, and Y.-W. Zhang, Nanoscale **8**, 483 (2016).
[34]Z. Ding, J.-W. Jiang, Q.-X. Pei, and Y.-W. Zhang, Nanotechnology **26**, 065703 (2015).
[35]X. Gu, B. Li, and R. Yang, J. Appl. Phys. **119**, 085106 (2016).
[36]J. J. Bae, H. Y. Jeong, G. H. Han, J. Kim, H. Kim, M. S. Kim, B. H. Moon, S. C. Lim, and Y. H. Lee, Nanoscale **9**, 2541 (2017).
[37]L. Lindsay, D. A. Broido, and N. Mingo, Phys. Rev. B **80**, 125407 (2009).
[38]M. Omini and A. Sparavigna, Phys. B: Phys. Condens. Matter **212**, 101 (1995).
[39]W. Li, J. Carrete, N. A. Katcho, and N. Mingo, Comput. Phys. Commun. **185**, 1747 (2014).
[40]L. Lindsay, D. A. Broido, and T. L. Reinecke, Phys. Rev. B **87**, 165201 (2013).
[41]L. Lindsay, D. A. Broido, and T. L. Reinecke, Phys. Rev. Lett. **109**, 095901 (2012).
[42]L. Lindsay, D. A. Broido, and T. L. Reinecke, Phys. Rev. Lett. **111**, 025901 (2013).
[43]G. Kresse and J. Furthmüller, Phys. Rev. B **54**, 11169 (1996).
[44]M. Dion, H. Rydberg, E. Schröder, D. C. Langreth, and B. I. Lundqvist, Phys. Rev. Lett. **92**, 246401 (2004).
[45]J. Klimeš, D. R. Bowler, and A. Michaelides, Phys. Rev. B **83**, 195131 (2011).
[46]A. K. Geim and I. V. Grigorieva, Nature **499**, 419 (2013).
[47]C. Bao, W. Yao, E. Wang, C. Chen, J. Avila, M. C. Asensio, and S. Zhou, Nano Lett. **17**, 1564 (2017).
[48]J. Dai and X. C. Zeng, J. Phys. Chem. Lett. **5**, 1289 (2014).
[49]J. E. Padilha, A. Fazzio, and A. J. R. da Silva, Phys. Rev. Lett. **114**, 066803 (2015).
[50]W. Hu, T. Wang, R. Zhang, and J. Yang, J. Mater. Chem. C **4**, 1776 (2016).
[51]J. Callaway, Phys. Rev. **113**, 1046 (1959).
[52]A. Ward, D. A. Broido, D. A. Stewart, and G. Deinzer, Phys. Rev. B **80**, 125203 (2009).
[53]L. Lindsay, D. A. Broido, and N. Mingo, Phys. Rev. B **82**, 161402 (2010).
[54]L. Lindsay, D. A. Broido, and N. Mingo, Phys. Rev. B **82**, 115427 (2010).
[55]L. Lindsay and D. A. Broido, J. Phys.: Condens. Matter. **20**, 165209 (2008).